Heliyon 9 (2023) e13219

Contents lists available at ScienceDirect

Heliyon

journal homepage: www.cell.com/heliyon

Research article

Metabolomics analysis of an AAA-ATPase Cdc48-deficient yeast strain

Tomoyuki Kawarasaki, Kunio Nakatsukasa *

Graduate School of Science, Nagoya City University, Yamanohata 1, Mizuho-cho, Mizuho-ku, Nagoya, Aichi, 467-8501, Japan

ARTICLE INFO

Keywords:
Citrate synthase
Glyoxylate cycle
Ubiquitin proteasome system
Cdc48/p97
Metabolome analysis
Saccharomyces cerevisiae

ABSTRACT

The ubiquitin-specific chaperone AAA-ATPase Cdc48 and its orthologs p97/valosin-containing protein (VCP) in mammals play crucial roles in regulating numerous intracellular pathways via segregase activity, which separates polyubiquitinated targets from membranes or binding partners. Interestingly, high-throughput experiments show that a vast number of metabolic enzymes are modified with ubiquitin. Therefore, Cdc48 may regulate metabolic pathways, for example by acting on the polyubiquitin chains of metabolic enzymes; however, the role of Cdc48 in metabolic regulation remains largely unknown. To begin to analyze the role of Cdc48 in metabolic regulation in yeast, we performed a metabolomics analysis of temperature-sensitive *cdc48-3* mutant cells. We found that the amount of metabolites in the glycolytic pathway was altered. Moreover, the pool of nucleotides, as well as the levels of metabolites involved in the tricarboxylic acid cycle and oxidative phosphorylation, increased, whereas the pool of amino acids decreased. These results suggest the involvement of Cdc48 in metabolic regulation in yeast. In addition, because of the roles of p97/VCP in regulating multiple cellular pathways, its inhibition is being considered as a promising anticancer drug target. We propose that the metabolomics study of Cdc48-deficient yeast will be useful as a complement to p97/VCP-related pathological and therapeutic studies.

1. Introduction

The AAA-ATPase Cdc48 in *Saccharomyces cerevisiae* and its orthologs p97/valosin-containing protein (VCP) in metazoans comprises an N-terminal domain, two centrally located ATPase domains, and a C-terminal tail. Six Cdc48 monomers form a double-ring structure surrounding a central pore [1,2]. This homohexameric structure, with the help of cofactors such as ubiquitin regulatory X (UBX) [3], exerts segregase activity, which separates ubiquitinated targets from membranes or binding partners. Thus, Cdc48 initiates the processing of diverse polyubiquitinated substrates by unfolding and translocating an attached ubiquitin molecule [4]. The role of Cdc48/p97 is best understood in the context of protein quality control, particularly during endoplasmic reticulum (ER)-associated degradation (ERAD) in which Cdc48/p97 mediates the delivery of ubiquitinated misfolded ER proteins to the proteasome [1,5–9]. Mutations in p97 can disrupt protein homeostasis and cause several neurodegenerative proteopathies [10–12]. The Cdc48 complex also reportedly segregates ubiquitinated protein aggregates and likely facilitates proteasomal degradation [13].

By its fundamental action on ubiquitinated proteins, Cdc48/p97 plays essential roles in diverse cellular processes, including chromosome segregation, mitotic spindle assembly, DNA repair, ER and Golgi formation, homotypic ER membrane fusion, ribosome-associated degradation, macroautophagy, ribophagy, cell wall integrity, telomerase regulation, NF-κB activation, regulation of

* Corresponding author.
E-mail address: nakatsukasa@nsc.nagoya-cu.ac.jp (K. Nakatsukasa).

https://doi.org/10.1016/j.heliyon.2023.e13219
Received 5 October 2022; Received in revised form 13 January 2023; Accepted 20 January 2023
Available online 24 January 2023

membrane-anchored transcription factors, and protein quality control [1,14–24]. Nevertheless, although recent systematic analyses have revealed that numerous metabolic enzymes, which are generally abundant in the cell compared with other proteins, are ubiquitinated, the functional links between Cdc48 and cellular metabolism remain unclear.

To analyze the role of Cdc48 in metabolic regulation, we first determined whether Cdc48 is involved in the degradation of a soluble metabolic enzyme, Cit2, a citrate synthase that functions in the gluconeogenic glyoxylate cycle in *S. cerevisiae*. In a previous study, we showed that Cit2 is a short-lived protein whose stability is regulated by proteasomal degradation mediated by the ubiquitin ligase complex SCF^{Ucc1} in cells grown in a glucose (to minimize the activity of the glyoxylate cycle) [25]. Here, we show that Cit2 degradation in temperature-sensitive *cdc48-3* mutant cells was slowed. As Cit2 was ubiquitinated robustly in *cdc48-3* mutant cells, we propose that Cdc48 acts at the post-ubiquitination step during Cit2 degradation. We then investigated the broader role of Cdc48 during metabolic regulation by performing a metabolomics analysis of *cdc48-3* cells. We found that the relative amounts of metabolites in the glycolytic pathway, tricarboxylic acid (TCA) cycle, and oxidative phosphorylation pathway in *cdc48-3* cells were different from those in wild-type cells. Moreover, the pool of nucleotides increased, while the pool of amino acids decreased. These results suggest the involvement of Cdc48 in metabolic regulation in yeast.

2. Experimental procedures

2.1. Strains and plasmids

The yeast strains used in this study are listed in Table 1. Yeast strain KNY494 was constructed as follows: a DNA fragment encoding *ucc1Δ::CgTRP* was amplified by PCR from p1805 (National BioResource Project, Japan) using primers OKN1718 (GTTTGTACTATGCCTATTGGCGCAAAGAAGACAGAGTGTGCAAACAAGAGGTTGTAAAACGACGGCCAGT) and OKN1719 (GCATAGACGTATATACACATATATTATAGACTAATTGATAAATTTTTTTTCAGGAAACAGCTATGACCAT). The resulting fragment was introduced into KNY140 [26] to generate KNY494. Correct integration was confirmed by colony PCR using primers OKN817 (TTCAAAGTCTCTGCCCCTCTATTG) and OKN818 (GTCAATAGGTACGATATAATGAGTGAGCTG). Cit2 was expressed from plasmid pKN404, which encodes *CIT2-HA-SKL* (the hemagglutinin tag is located upstream of the peroxisomal targeting signal at the C-terminus) under control of the *CIT2* promoter. pKN404 was constructed as follows: pKN194 [25] was digested with SacI/XhoI and the resulting fragment was inserted into the same sites of pRS316 [27]. Next, pRS423mycUb (*2μ* HIS3) was used to express 6 × His-tagged myc-Ub under control of the *CUP1* promoter [28].

2.2. Culture conditions

Yeast cells were grown in YPD medium (1% yeast extract, 1% peptone, 100 mg/L adenine hydrochloride, and 2% glucose) or SD medium (0.67% yeast nitrogen base without amino acids, 100 mg/L adenine hydrochloride, all standard amino acids, and 2% glucose). Appropriate amino acids were excluded from synthetic medium to maintain plasmids.

2.3. Antibodies

Polyclonal anti-Cdc48 antibodies were a generous gift from T. Endo (Kyoto Sangyo University) and were diluted into TBS-T buffer (20 mM Tris-HCl, pH 7.5, 150 mM NaCl, and 0.1% Tween-20) at ~1/20,000. An anti-HA antibody (#M180-3) was purchased from MBL and was diluted into TBS-T buffer at 1/10,000. Anti-mouse IgG-HRP (#A4416-1 ML) and anti-rabbit IgG-HRP (#A6154-1 ML)

Table 1
Strains used in this study.

Genotype	Source	Name
*MAT***a** *ade2-1 ura3-1 his3-11,15 trp1-1 leu2-3112 can1-100*	Y. Kikuchi	W303-1a
*MAT***a** *his3Δ1 leu2Δ0 met15Δ0 ura3Δ0*	S. Michaelis	BY4741
*MAT***a** *ade2-1 ura3-1 his3-11,15 trp1-1 leu2-3112 can1-100 pdr5::HYH, pep4::LEU2*	(Nakatsukasa et al., 2013)	KNY140
*MAT***a** *ade2-1 ura3-1 his3-11,15 trp1-1 leu2-3112 can1-100 pdr5::HYH, pep4::LEU2, cdc48-3*	(Nakatsukasa et al., 2013)	KNY208
*MAT***a** *ade2-1 ura3-1 his3-11,15 trp1-1 leu2-3112 can1-100 pdr5::HYH, pep4::LEU2, ucc1::CgTRP*	This study	KNY494
*MAT***a** *his3Δ1 leu2Δ0 met15Δ0 ura3Δ0 ucc1::KanR*	Open biosystems	N/A
*MAT***a** *his3Δ1 leu2Δ0 met15Δ0 ura3Δ0 ubx2::KanR*	Open biosystems	N/A
*MAT***a** *his3Δ1 leu2Δ0 met15Δ0 ura3Δ0 ubx3::KanR*	Open biosystems	N/A
*MAT***a** *his3Δ1 leu2Δ0 met15Δ0 ura3Δ0 ubx4::KanR*	Open biosystems	N/A
*MAT***a** *his3Δ1 leu2Δ0 met15Δ0 ura3Δ0 ubx5::KanR*	Open biosystems	N/A
*MAT***a** *his3Δ1 leu2Δ0 met15Δ0 ura3Δ0 ubx6::KanR*	Open biosystems	N/A
*MAT***a** *his3Δ1 leu2Δ0 met15Δ0 ura3Δ0 ubx7::KanR*	Open biosystems	N/A
*MAT***a** *his3Δ1 leu2Δ0 met15Δ0 ura3Δ0 ufd2::KanR*	Open biosystems	N/A
*MAT***a** *his3Δ1 leu2Δ0 met15Δ0 ura3Δ0 ufd3::KanR*	Open biosystems	N/A
*MAT***a** *his3Δ1 leu2Δ0 met15Δ0 ura3Δ0 otu1::KanR*	Open biosystems	N/A
*MAT***a** *his3Δ1 leu2Δ0 met15Δ0 ura3Δ0 vms1::KanR*	Open biosystems	N/A

Nakatsukasa K, Brodsky JL & Kamura T (2013) A stalled retrotranslocation complex reveals physical linkage between substrate recognition and proteasomal degradation during ER-associated degradation. *Mol Biol Cell* **24**: 1765–1775, S1761-1768.

were obtained from Sigma-Aldrich, diluted into TBS-T buffer at 1/7,000, and used as secondary antibodies. A mono- and poly-ubiquitinated conjugated/mouse mAb horseradish peroxidase conjugate (FK2H) (#PW0150) was obtained from BioMol.

2.4. Immunoblotting

Immunoblotting was performed essentially as described previously [29]. Proteins were separated on SDS–PAGE gel and transferred to a PVDF membrane (Immobilon-P, MERCK). The membrane was washed with TBS-T buffer briefly and incubated overnight at 4 °C with a primary antibody solution. The membrane was washed with TBS-T buffer for 90 min, incubated with a secondary antibody solution for 60 min at room temperature, and washed with TBS-T buffer for more than 90 min. The membrane was then incubated with Chemi-Lumi One (#07880, Nacalai Tesque) or Luminata Forte Western HRP substrate (#WBLUF0500, Millipore) and exposed to X-ray film. ImageJ (National Institute of Health) was used for quantification of western blot images and CBB-stained membranes.

2.5. Cycloheximide chase assay

The cycloheximide chase assay was performed essentially as described [25,29,30]. Typically, yeast cells were grown to logarithmic phase. The *cdc48-3* temperature-sensitive strains were grown at 26 °C and shifted to 37 °C for 2 h. The culture (~5 mL) was harvested and mixed with 30 mM NaN_3. Cells were pelleted by centrifugation and stored at −80 °C. This sample was designated as time = 0. Subsequently, cycloheximide (#06741-04, Nacalai Tesque) was added to the remaining culture at a final concentration of 100–250 μg/mL. At the indicated time points, the same volume of culture was harvested, mixed with 30 mM NaN_3, and collected by centrifugation. The cell pellet was stored at −80 °C. The frozen cell pellet was then suspended in 300 μL of 20% trichloroacetic acid (TCA) and disrupted by vigorous vortexing (Max Mixer EVR-032, TAITEC) in the presence of glass beads (YGBLA-05, Yasui Kikai). The cell lysate was added to 900 μL of 5% TCA, and 1000 μL of the suspension was transferred to a new tube. Proteins were precipitated by centrifugation at 20,000 g for 15 min at 4 °C. The precipitates were dissolved in KNTCASB (80 mM Tris-HCl, pH 7.5, 8 mM EDTA, pH 8.0, 12.5% glycerol, 8 M urea, 4% SDS, 200 mM DTT, 0.8 mg/mL Tris, and 0.1% BPB) by vigorous vortexing for ~30 min, heated at 55 °C for 15 min, centrifuged at 20,000 g for 1 min at room temperature, and analyzed by SDS–PAGE.

2.6. In vivo ubiquitination assay

Cells expressing Cit2-HA were transformed with plasmid pRS423mycUb (*2μ*, *HIS3*, P_{CUP1}-*6xHIS tagged Ub*) [28]. The cells were then cultured overnight in synthetic complete medium and diluted 50–100-fold in a fresh medium. Expression of His-tagged Ubiquitin was induced by addition of 100 μM $CuSO_4$ to the medium for 5–8 h before cells were collected and stored at −80 °C. Typically, ~50 OD_{600} cells were collected. Cells in 250 μL of buffer (20 mM Tris-HCl, pH 7.5, 150 mM NaCl, 0.5% Triton X-100, 0.1% SDS, 10 mM N-ethylmaleimide) were placed in a round bottom plastic tube and lysed using glass beads (eight rounds of vigorous vortexing for 30 s with 30 s intervals on ice). The same buffer (500 μL) was added again, and the suspension was transferred to a new tube. The glass beads were washed once again with 500 μL of buffer and pooled in the same tube. The collected lysates were cleared by centrifugation at 20,000 g for 10 min at 4 °C. The cleared lysates were incubated overnight at 4 °C with 1 μL of anti-HA antibody and Dynabeads Protein G (Invitrogen). The beads were then washed four times with buffer (20 mM Tris-HCl, pH 7.5, 150 mM NaCl, 0.5% Triton X-100, 0.05% SDS, 10 mM N-ethylmaleimide). Immunoprecipitated proteins were eluted for 30 min at 55 °C with KNTCASB, separated by SDS–PAGE, and subjected to western blotting. The extent of the polyubiquitin chains was detected with a mono- and polyubiquitinated conjugated/mouse mAb horseradish peroxidase conjugate (FK2H).

2.7. Metabolome analysis

Cells (20 OD_{600} equivalent) were collected by centrifugation and washed twice with Milli-Q water. The cells were treated with 1600 μL of methanol by ultrasonication for 30 s to inactivate enzymes. Next, the cell extract was treated with 1100 μL of Milli-Q water containing internal standards (H3304-1002, Human Metabolome Technologies, (HMT), Tsuruoka, Yamagata, Japan) and left at rest for another 30 s. The extract was obtained and centrifuged for 5 min at 2300×*g* at 4 °C. Next, 1400 μL of the upper aqueous layer was centrifugally filtered for 120 min through a Millipore 5-kDa cut-off filter (9100×*g* and 4 °C) to remove proteins. The filtrate was concentrated by centrifugation and re-suspended in 50 μL of Milli-Q water for CE-MS analysis. Metabolome measurements were carried out by a facility service at HMT Inc., Tsuruoka, Japan. Metabolome analysis was conducted using the Basic Scan package of HMT and capillary electrophoresis time-of-flight mass spectrometry (CE-TOFMS), based on methods described previously [31,32]. Briefly, CE-TOFMS analysis was carried out using an Agilent CE capillary electrophoresis system equipped with an Agilent 6210 time-of-flight mass spectrometer (Agilent Technologies, Waldbronn, Germany). The systems were controlled by Agilent G2201AA ChemStation software version B.03.01 for CE (Agilent Technologies), and connected by a fused silica capillary (50 μm i.d. × 80 cm total length). Commercial electrophoresis buffer (H3301-1001 and I3302-1023 for cation and anion analyses, respectively, HMT) was used as the electrolyte. The spectrometer was scanned from *m/z* 50 to 1000 [31]. Peaks were extracted using MasterHands automatic integration software (Keio University, Tsuruoka, Yamagata, Japan) [33] and MassHunter Quantitative Analysis B.04.00 (Agilent Technologies) to obtain peak information, including *m/z*, peak area, and migration time (MT). Signal peaks were annotated according to the HMT metabolite database based on their *m/z* values and MTs. The areas of the annotated peaks were normalized to internal standard levels and sample amounts to obtain relative levels for each metabolite. Primary (n = 110) metabolites were quantified absolutely based on one-point calibrations using their respective standard compounds. Hierarchical cluster analysis and principal

component analysis (PCA) were performed by HMT's proprietary software, PeakStat and SampleStat, respectively. Detected metabolites were plotted on metabolic pathway maps using VANTED software [34].

3. Results

3.1. Degradation of Cit2 depends on Cdc48 and its cofactor Ubx4

To investigate whether Cdc48 is involved in Cit2 degradation, we inactivated Cdc48 using the widely used temperature-sensitive

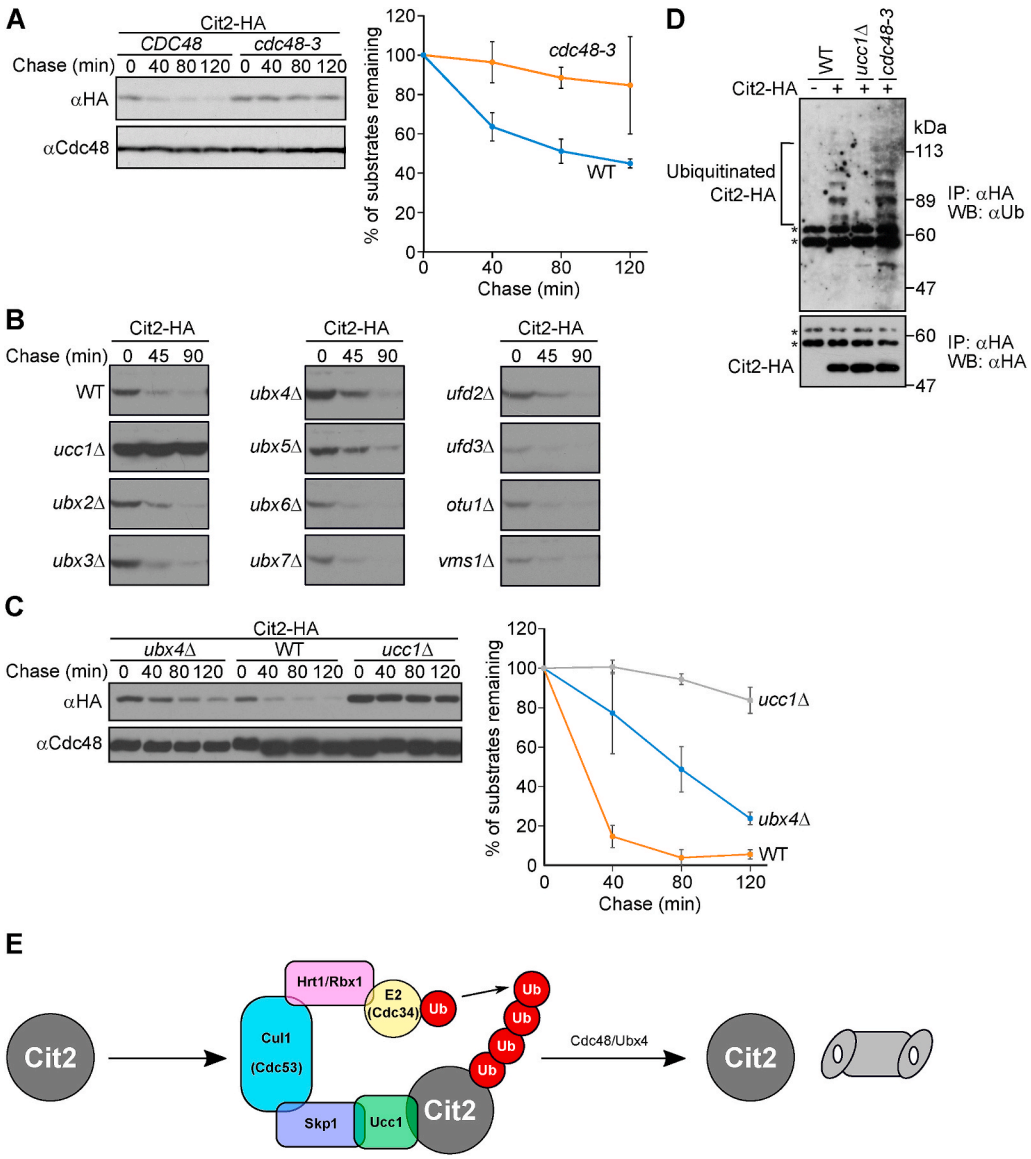

Fig. 1. Cit2 degradation is slowed in *cdc48-3* cells. (A) Cycloheximide chase analysis of Cit2-HA in temperature-sensitive *cdc48-3* mutant cells. Cells were grown to mid-log phase at 26 °C and then shifted to 37 °C for 2 h prior to addition of cycloheximide. Samples were taken at the indicated time points and lysates were prepared. Proteins were separated by SDS–PAGE and immunoblotted with an anti-HA antibody. Cdc48 was used as a loading control. (B) Cycloheximide chase analysis of Cit2-HA in the indicated mutant strains. Cells were grown to the mid-log phase at 30 °C and processed as in (A). (C) Cycloheximide chase analysis of Cit2-HA in the indicated mutant strains. Cells were grown to the mid-log phase at 30 °C and then processed as in (A). Cdc48 was used as a loading control. Data represent the mean ± SE of three independent experiments. (D) The *in vivo* ubiquitination status of Cit2-HA was analyzed in the indicated strains. See Materials and methods for details. In brief, cells expressing Cit2-HA were cultured overnight and the expression of His-tagged ubiquitin was induced by 100 μM of $CuSO_4$ for 5–8 h. Cells were collected and lysed with glass beads. The resulting lysates were cleared by centrifugation at 15,000 rpm for 10 min at 4 °C and subjected to immunoprecipitation with an anti-HA antibody. The polyubiquitin chains on Cit2-HA were detected with an anti-Ub antibody. Asterisks indicate IgG and/or non-specific bands. IP, immunoprecipitation; WB, western blotting. Uncropped blots or a substantial portion of the blots are presented in Supplementary Fig. S2.

mutant *cdc48-3* cells [26,35] and performed cycloheximide chase analysis. After the cells were treated with cycloheximide, Cit2 in wild-type cells was readily degraded, while it was almost completely stable in *cdc48-3* cells (Fig. 1A), suggesting that Cdc48 is involved in Cit2 degradation. We also examined the involvement of a series of Cdc48 cofactors in Cit2 degradation. While deletion of *UCC1* inhibited Cit2 degradation almost completely, deletion of *UBX4* moderately but reproducibly stabilized Cit2 (Fig. 1B and C). We then further analyzed the ubiquitination status of Cit2 in *cdc48-3* cells. Cit2 was immunoprecipitated with an anti-HA antibody under denaturing conditions (see Materials and methods) and the precipitated proteins were subjected to immunoblotting with an anti-ubiquitin antibody. As shown in Fig. 1D, Cit2 in *cdc48-3* cells was ubiquitinated to a similar extent as in isogenic wild-type cells. These results suggest that the Cdc48-Ubx4 complex contributes to Cit2 degradation, most likely at the post-ubiquitination step (Fig. 1E).

3.2. Metabolomic profiling of cdc48-3 cells

To investigate the general role of Cdc48 in metabolic regulation, we analyzed the metabolomics profiles of *cdc48-3* cells. A total of 231 metabolites (128 and 103 metabolites in the cation and anion modes, respectively) were detected (Supplementary Tables S1 and S2). These metabolites were involved in glycolysis, the TCA cycle, oxidative phosphorylation, amino acid metabolism, and nucleotide metabolism. Principal component analysis (PCA) was performed to compare the overall metabolomics profiles (Fig. 2A; Supplementary Tables S3 and S4). In essence, PCA showed good clustering of metabolomic changes related to Cdc48 inactivation. Hierarchical clustering analysis was then performed to study the metabolomics profiles of wild-type and *cdc48-3* cells. The heat map representation of metabolomics profiles analyzed with hierarchical clustering analysis is summarized in Fig. 2B (with complete data in Supplementary Table S5). In this analysis, the level of several metabolites in *cdc48-3* cells increased or decreased (see Supplementary Table S5). A relative comparison of target metabolites in wild-type and *cdc48-3* cells, superimposed on a possible metabolic pathway map, is shown in Supplementary Fig. S1.

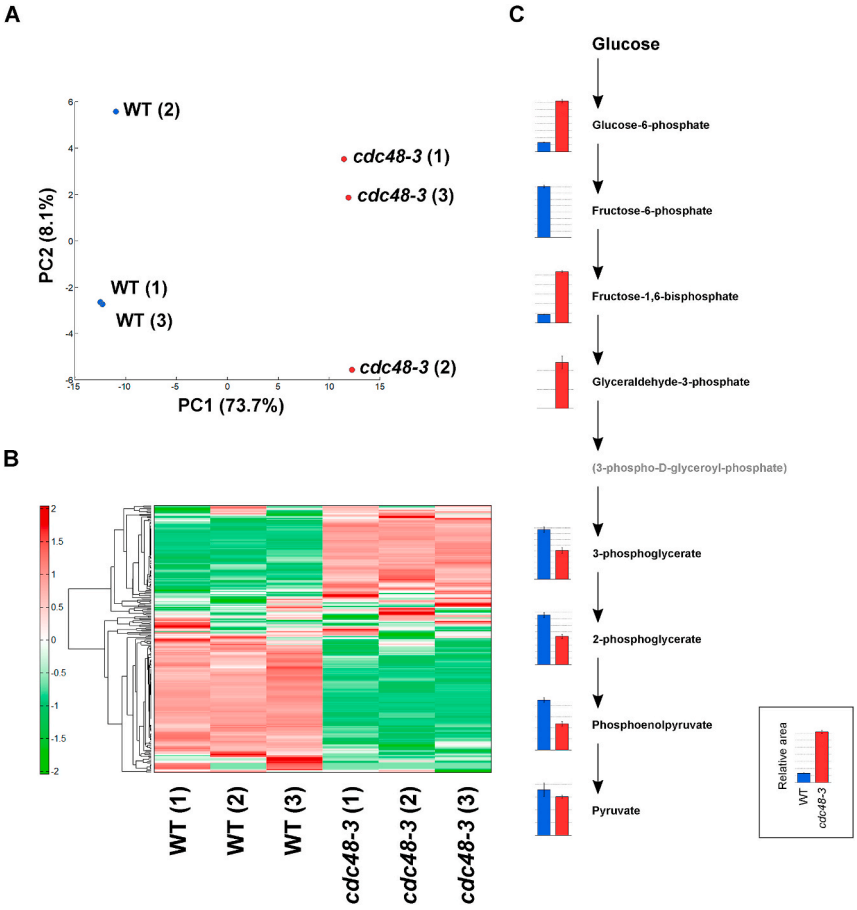

Fig. 2. Principal component analysis, hierarchical clustering analysis, and relative amounts of metabolites in the glycolytic pathway in *cdc48-3* cells. (A) Principal component 1 (PC1) versus principal component 2 (PC2) plot based on the results of principal component analysis. (B) Heat map representation of the metabolomics profiles analyzed by hierarchical clustering analysis. (C) The relative amounts of metabolites in the glycolytic pathway of wild-type and *cdc48-3* cells are shown as a bar graph.

Table 2
Relative amounts of select metabolites in wild-type and *cdc48-3* cells.

A	ID	Compound name	KEGG ID	*m/z*	MT/RT	Relative Area										Comparative Analysis		
						wild type			*cdc48-3*			wild type		*cdc48-3*		*cdc48-3* vs wild type		
						A1	A2	A3	B1	B2	B3	Mean	S.D.	Mean	S.D.	Ratio¶	*p-value*‖	
	A_0057	Glucose 6-phosphate	C00668, C01172, C00092	259.023	9.90	6.4E-03	7.0E-03	6.4E-03	3.5E-02	3.7E-02	3.6E-02	6.6E-03	3.6E-04	3.6E-02	1.2E-03	5.4334	0.000244	***
	A_0058	Fructose 6-phosphate	C05345, C00085	259.023	10.00	4.1E-03	3.9E-03	4.0E-03	N.D.	N.D.	N.D.	4.0E-03	1.2E-04	N.A.	N.A.	<1	N.A.	
	A_0071	Fructose 1,6-diphosphate	C00354	338.990	14.62	1.7E-02	1.8E-02	1.8E-02	1.0E-01	1.1E-01	1.1E-01	1.8E-02	7.4E-04	1.1E-01	2.5E-03	6.0188	0.000081	***
	A_0031	Glyceraldehyde 3-phosphate	C00118, C00661	168.991	11.66	N.D.	N.D.	N.D.	1.4E-03	1.2E-03	1.1E-03	N.A.	N.A.	1.2E-03	1.7E-04	1<	N.A.	
	A_0039	3-Phosphoglyceric acid	C00197	184.986	19.64	4.3E-02	4.1E-02	4.6E-02	2.8E-02	2.3E-02	2.4E-02	4.4E-02	2.6E-03	2.5E-02	2.6E-03	0.5811	0.000966	***
	A_0040	2-Phosphoglyceric acid	C00631	184.986	19.17	8.1E-03	7.3E-03	7.4E-03	4.7E-03	4.2E-03	4.1E-03	7.6E-03	4.3E-04	4.3E-03	3.3E-04	0.5699	0.000651	***
	A_0030	Phosphoenolpyruvic acid	C00074	166.976	21.00	2.1E-02	2.3E-02	2.3E-02	1.3E-02	1.1E-02	1.2E-02	2.2E-02	1.1E-03	1.2E-02	1.0E-03	0.5243	0.000263	***
	A_0004	Pyruvic acid	C00022	87.009	12.91	1.6E-02	1.7E-02	2.1E-02	1.5E-02	1.5E-02	1.6E-02	1.8E-02	2.6E-03	1.5E-02	5.7E-04	0.8487	0.209150	

B	ID	Compound name	KEGG ID	*m/z*	MT/RT	Relative Area										Comparative Analysis		
						wild type			*cdc48-3*			wild type		*cdc48-3*		*cdc48-3* vs wild type		
						A1	A2	A3	B1	B2	B3	Mean	S.D.	Mean	S.D.	Ratio¶	*p-value*‖	
	A_0043	Isocitric acid	C00311	191.019	28.49	3.0E-03	N.D.	3.6E-03	3.4E-03	4.4E-03	4.0E-03	3.3E-03	4.4E-04	3.9E-03	4.9E-04	1.1858	0.254070	
	A_0019	Malic acid	C00149, C00497, C00711	133.015	21.20	1.5E-01	1.5E-01	1.5E-01	3.3E-01	3.2E-01	3.3E-01	1.5E-01	1.7E-03	3.3E-01	5.2E-03	2.1558	0.000079	***
	A_0016	Succinic acid	C00042	117.020	20.78	1.4E-01	1.4E-01	1.5E-01	2.4E-01	2.2E-01	2.5E-01	1.4E-01	6.4E-03	2.4E-01	1.1E-02	1.6325	0.000693	***
	A_0092	ADP	C00008	426.023	10.93	1.3E-01	1.3E-01	1.4E-01	1.1E-01	9.9E-02	1.0E-01	1.3E-01	6.3E-03	1.0E-01	4.4E-03	0.7704	0.003398	**
	A_0105	ATP	C00002	505.990	11.85	2.3E-01	2.3E-01	2.4E-01	3.4E-01	3.4E-01	3.6E-01	2.3E-01	7.2E-03	3.5E-01	7.0E-03	1.4983	0.000037	***
	A_0112	NAD+	C00003	662.104	6.65	2.5E-01	2.5E-01	2.5E-01	2.5E-01	2.3E-01	2.4E-01	2.5E-01	8.8E-04	2.4E-01	9.3E-03	0.9702	0.301370	
	A_0113	NADH	C00004	664.120	8.25	9.5E-03	9.5E-03	1.0E-02	1.3E-02	1.4E-02	1.4E-02	9.8E-03	4.8E-04	1.4E-02	4.7E-04	1.3813	0.000641	***

C	ID	Compound name	KEGG ID	*m/z*	MT/RT	Relative Area										Comparative Analysis		
						wild type			*cdc48-3*			wild type		*cdc48-3*		*cdc48-3* vs wild type		
						A1	A2	A3	B1	B2	B3	Mean	S.D.	Mean	S.D.	Ratio¶	*p-value*‖	
	C_0004	Ala	C00041, C00133, C01401	90.055	8.83	3.1E+00	3.1E+00	3.2E+00	1.9E+00	2.1E+00	2.0E+00	3.1E+00	4.4E-02	2.0E+00	7.5E-02	0.6353	0.000110	***
	C_0040	Arg	C00062, C00792	175.119	6.91	1.5E+00	1.6E+00	1.7E+00	1.5E+00	1.6E+00	1.6E+00	1.6E+00	1.1E-01	1.6E+00	4.6E-02	1.0109	0.814850	

(*continued on next page*)

Table 2 (*continued*)

C	ID	Compound name	KEGG ID	*m/z*	MT/RT	Relative Area										Comparative Analysis		
						wild type			*cdc48-3*			wild type		*cdc48-3*		*cdc48-3* vs wild type		
						A1	A2	A3	B1	B2	B3	Mean	S.D.	Mean	S.D.	Ratio[¶]	*p-value*[‖]	
	C_0025	Asn	C00152, C01905, C16438	133.061	10.31	4.3E-01	4.5E-01	4.6E-01	3.1E-01	3.4E-01	3.1E-01	4.5E-01	1.2E-02	3.2E-01	1.8E-02	0.7119	0.000830	***
	C_0027	Asp	C00049, C00402, C16433	134.045	11.41	2.5E+00	2.5E+00	2.5E+00	9.0E-01	9.4E-01	9.0E-01	2.5E+00	3.3E-02	9.1E-01	2.7E-02	0.3689	0.000001	***
	C_0019	Cys	C00097, C00736, C00793	122.027	11.17	1.9E-03	1.5E-03	2.3E-03	1.1E-03	9.1E-04	9.9E-04	1.9E-03	4.0E-04	9.9E-04	8.2E-05	0.5184	0.051546	
	C_0033	Gln	C00064, C00303, C00819	147.076	10.57	2.3E+00	2.4E+00	2.5E+00	3.5E+00	3.9E+00	3.6E+00	2.4E+00	9.0E-02	3.7E+00	1.8E-01	1.5538	0.001801	**
	C_0035	Glu	C00025, C00217, C00302	149.064	10.69	7.4E-01	7.5E-01	7.5E-01	6.5E-01	7.1E-01	6.5E-01	7.5E-01	8.7E-03	6.7E-01	3.6E-02	0.8943	0.055789	
	C_0001	Gly	C00037	76.039	8.13	7.7E-01	7.7E-01	8.4E-01	7.1E-01	7.4E-01	7.2E-01	7.9E-01	3.9E-02	7.2E-01	1.1E-02	0.9132	0.082860	
	C_0038	His	C00135, C00768, C06419	156.077	7.10	1.7E+00	1.8E+00	1.9E+00	1.1E+00	1.2E+00	1.1E+00	1.8E+00	1.2E-01	1.1E+00	3.7E-02	0.6397	0.006336	**
	C_0023	Ile	C00407, C06418, C16434	132.102	10.07	7.2E-01	7.6E-01	7.8E-01	5.1E-01	5.1E-01	5.1E-01	7.5E-01	2.9E-02	5.1E-01	3.1E-03	0.6764	0.004439	**
	C_0024	Leu	C00123, C01570, C16439	132.102	10.17	1.7E+00	1.6E+00	1.7E+00	8.2E-01	8.5E-01	8.3E-01	1.7E+00	4.9E-02	8.4E-01	1.7E-02	0.5052	0.000366	***
	C_0034	Lys	C00047, C00739, C16440	148.116	6.62	6.2E-01	6.4E-01	6.7E-01	3.2E-01	3.3E-01	3.2E-01	6.4E-01	2.5E-02	3.3E-01	4.4E-03	0.5054	0.001625	**
	C_0036	Met	C00073, C00855, C01733	150.059	10.54	2.8E-01	2.8E-01	2.9E-01	1.4E-01	1.5E-01	1.4E-01	2.8E-01	4.0E-03	1.4E-01	2.5E-03	0.5086	0.000005	***
	C_0039	Phe	C00079, C02057, C02265	166.086	10.94	7.3E-01	7.4E-01	7.6E-01	3.2E-01	3.5E-01	3.4E-01	7.4E-01	1.5E-02	3.4E-01	1.4E-02	0.4569	0.000005	***
	C_0013	Pro	C00148, C00763, C16435	116.071	10.65	8.2E-01	8.5E-01	8.0E-01	7.7E-01	8.2E-01	7.7E-01	8.2E-01	2.8E-02	7.9E-01	2.8E-02	0.9566	0.192940	
	C_0009	Ser	C00065, C00716, C00740	106.050	9.81	7.0E-01	7.2E-01	7.4E-01	7.2E-01	7.7E-01	7.1E-01	7.2E-01	1.9E-02	7.3E-01	3.3E-02	1.0177	0.601030	
	C_0017	Thr	C00188, C00820	120.066	10.35	1.3E+00	1.3E+00	1.3E+00	9.9E-01	1.0E+00	9.8E-01	1.3E+00	4.9E-02	1.0E+00	3.1E-02	0.7765	0.002050	**
	C_0044	Trp	C00078, C00525, C00806	205.097	10.80	1.1E-02	1.0E-02	1.2E-02	8.4E-03	9.2E-03	8.8E-03	1.1E-02	7.2E-04	8.8E-03	3.6E-04	0.7815	0.014066	*

(*continued on next page*)

Table 2 (*continued*)

C	ID	Compound name	KEGG ID	*m/z*	MT/RT	Relative Area										Comparative Analysis		
						wild type			*cdc48-3*			wild type		*cdc48-3*		*cdc48-3* vs wild type		
						A1	A2	A3	B1	B2	B3	Mean	S.D.	Mean	S.D.	Ratio¶	*p-value*||	
	C_0042	Tyr	C00082, C01536, C06420	182.082	11.22	8.6E-02	8.7E-02	9.4E-02	8.2E-02	8.8E-02	8.1E-02	8.9E-02	4.5E-03	8.4E-02	3.7E-03	0.9400	0.192220	
	C_0014	Val	C00183, C06417, C16436	118.086	9.87	1.4E+00	1.5E+00	1.5E+00	1.0E+00	1.1E+00	1.0E+00	1.5E+00	4.2E-02	1.0E+00	2.6E-02	0.6949	0.000301	***

D	ID	Compound name	KEGG ID	*m/z*	MT/RT	Relative Area										Comparative Analysis		
						wild type			*cdc48-3*			wild type		*cdc48-3*		*cdc48-3* vs wild type		
						A1	A2	A3	B1	B2	B3	Mean	S.D.	Mean	S.D.	Ratio¶	*p-value*||	
	A_0107	GTP	C00044	521.985	11.53	4.6E-02	4.6E-02	5.0E-02	7.4E-02	7.5E-02	7.8E-02	4.7E-02	2.4E-03	7.6E-02	2.0E-03	1.5999	0.000111	***
	A_0101	CTP	C00063	481.980	12.42	1.7E-02	1.8E-02	1.7E-02	3.4E-02	3.3E-02	3.6E-02	1.7E-02	6.6E-04	3.4E-02	1.3E-03	1.9569	0.000303	***
	A_0104	dATP	C00131	489.996	11.80	4.8E-03	4.7E-03	4.7E-03	9.9E-03	9.6E-03	1.0E-02	4.8E-03	6.3E-05	9.9E-03	3.9E-04	2.0859	0.001461	**
	A_0100	dTTP	C00459	480.984	12.17	6.0E-03	5.1E-03	5.6E-03	1.4E-02	1.4E-02	1.3E-02	5.5E-03	4.5E-04	1.4E-02	7.3E-04	2.4781	0.000264	***
	A_0106	dGTP	C00286	505.991	11.54	1.6E-03	1.5E-03	1.7E-03	2.8E-03	2.8E-03	3.1E-03	1.6E-03	1.0E-04	2.9E-03	1.6E-04	1.8463	0.000698	***
	A_0099	dCTP	C00458	465.984	12.50	2.6E-03	2.8E-03	2.7E-03	7.0E-03	7.2E-03	7.6E-03	2.7E-03	1.2E-04	7.3E-03	3.4E-04	2.6934	0.000653	***

ID consists of analysis mode and number. 'C' and 'A' showed cation and anion modes, respectively.
N.D. (Not Detected): The target peak or metabolite was below detection limits.
N.A. (Not Available): The calculation was impossible because of insufficience of the data.
¶ The ratio is of computed by using averaged detection values. The latter was used as denominator.
|| The p-value is computed by Welch's *t*-test. (*<0.05, **<0.01, ***<0.001).
Glu, Lys: Peak intensity is saturated. Relative area was computed by using 13C isotope ion peak.

3.3. Relative amounts of metabolites in specific metabolic pathways in wild-type and cdc48-3 cells

The relative amounts of metabolites in the glycolytic pathway of wild-type and *cdc48-3* cells are summarized in Fig. 2C and Table 2A. In the first half of the glycolytic pathway, there was a significant accumulation of glucose-6-phosphate, fructose-1,6-bisphosphate, and glyceraldehyde-3-phosphate in *cdc48-3* cells compared with wild-type cells, whereas higher amounts of fructose-6-phosphate were observed in wild-type cells than in *cdc48-3* cells. In contrast, in the latter half of the glycolytic pathway, metabolites were less abundant (~50%) in *cdc48-3* cells compared with wild-type cells.

The relative amounts of metabolites in the TCA cycle and oxidative phosphorylation in wild-type and *cdc48-3* cells are summarized in Fig. 3A and Table 2B. The levels of isocitrate (1.2-fold, but statistically non-significant), succinate (1.6-fold), fumarate (2.1-fold), malate (2.2-fold), ATP (1.5-fold), and NADH (1.4-fold) increased in *cdc48-3* cells. In contrast, the levels of acetyl-CoA (0.6-fold), citrate (0.7-fold), and ADP (0.8-fold) decreased, while that of NAD^+ (0.97-fold) was unchanged. The reason for the lower levels of acetyl-CoA and citrate in *cdc48-3* cells is currently unclear, but the observed accumulation of ATP suggests that the TCA cycle and oxidative phosphorylation in mitochondria may be more active in *cdc48-3* cells than in wild-type cells.

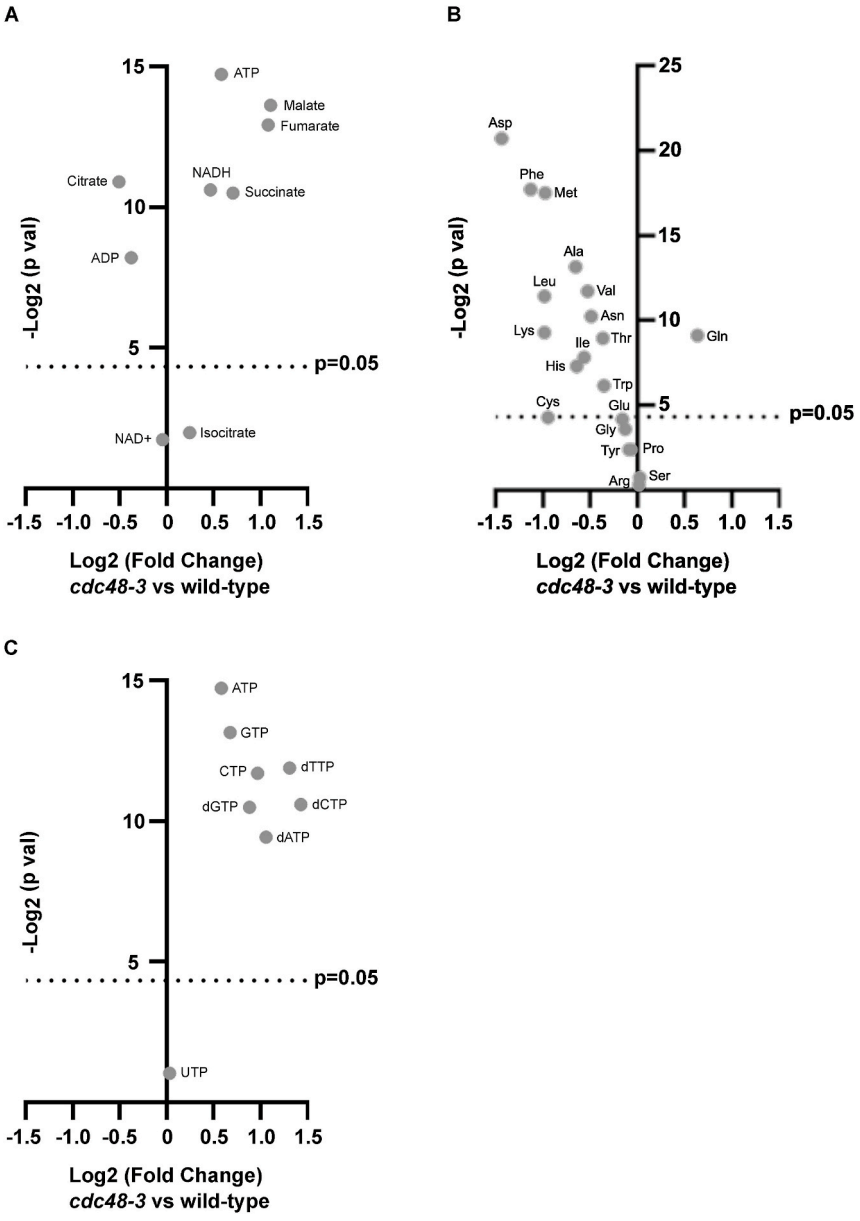

Fig. 3. Changes in the abundance of select metabolites in *cdc48-3* cells. (A–C) Volcano plot showing the relative amounts of metabolites involved in the TCA cycle and oxidative phosphorylation (A), as well as relative amounts of amino acids (B), and nucleotides (C), in *cdc48-3* cells.

The relative amounts of amino acids in wild-type and *cdc48-3* cells are summarized in Fig. 3B and Table 2C. Except for glutamine, the levels of most amino acids in *cdc48-3* cells were lower than those in wild-type cells. One possible explanation for this phenomenon is that Cdc48 inactivation results in the accumulation of ubiquitinated degradation substrates, leading to an inefficient supply of degradation products, including amino acids.

The relative amounts of nucleotides in wild-type and *cdc48-3* cells are summarized in Fig. 3C and Table 2D. We observed an increase in the levels of ATP (1.5-fold), GTP (1.6-fold), CTP (2.0-fold), dATP (2.1-fold), dGTP (1.8-fold), dTTP (2.5-fold), and dCTP (2.7-fold), while the level of UTP (1.0-fold) was almost unchanged. One possible explanation for this is that Cdc48 inactivation alters the activity of enzymes involved in nucleotide biosynthesis. A global cellular phenotype resulting from *cdc48-3* mutation could also be another reason for these changes (see Discussion).

4. Discussion

In the first part of this study, we demonstrated that the degradation of Cit2, a citrate synthase in the gluconeogenic glyoxylate cycle of yeast, depends on Cdc48 and Ubx4. Although it is now clear that Cit2 degradation is significantly slowed in *cdc48-3* cells, the mechanism by which Cdc48 facilitates Cit2 degradation remains unclear. Previous studies have shown that Ubx4 is involved in ERAD, the degradation of fructose-1,6-bisphosphatase (FBPase: a key enzyme in the gluconeogenic pathway), and the UV-dependent turnover of RNA polymerase II [36ndash;39]. In addition, Cdc48-Ubx4 is crucial for the nuclear distribution of the 26S proteasome [40]. In all cases, Cdc48-Ubx4 is supposed to act at the post-ubiquitination step. Even in the case of Cit2 degradation, Cdc48-Ubx4 likely functions at the post-ubiquitination step because Cit2 was robustly ubiquitinated in *cdc48-3* cells (Fig. 1D). In general, citrate synthase needs to form a stable dimer for its activity [41]. Therefore, one possible scenario is that Cdc48-Ubx4 associates with the polyubiquitin chain on the Cit2 dimer, and disassembles it for efficient proteasomal degradation. Cdc48-Ubx4 may also facilitate the transport of ubiquitinated Cit2 to the proteasome. In mammals, a similar function of p97/VCP has been observed during the degradation of glutamine synthetase downstream of CRBN, the target of so-called immunomodulatory drugs [42]. However, it is also possible that the slowed degradation of Cit2 in *cdc48-3* cells might be a result of global changes in proteostasis, which was caused by the disturbance of protein quality control and organelle homeostasis [43]. Thus, it will be important to clarify whether Cdc48 directly or indirectly facilitates Cit2 degradation.

We previously demonstrated that oxaloacetate can induce a conformational change in Cit2 and inhibit its recognition via Ucc1, thereby stabilizing Cit2 [25]. Based on this observation, we proposed that the Ucc1-mediated degradation of Cit2 acts as a metabolic switch for the glyoxylate cycle [25]. One might assume that Cdc48 inactivation results in Cit2 stabilization, and thereby causing the accumulation of citrate. However, while Cdc48 regulates Cit2 stability, it also regulates many other cellular metabolic processes. Indeed, citrate level was rather decreased in cdc48-3 cells (Fig. 3A, Table 2B). This may be due to the global alteration of metabolism resulting from Cdc48 inactivation.

In the second part of this study, we performed a metabolomics analysis of *cdc48-3* cells. The amount of metabolites in the central carbon pathway was altered in *cdc48-3* cells (Fig. 2C). In particular, the levels of metabolites involved in the TCA cycle and oxidative phosphorylation increased, and nucleotides accumulated. However, the pool of amino acids decreased (Fig. 3). Currently, it is unknown whether these results are due to the action of Cdc48 on polyubiquitinated metabolic enzymes or a global cellular phenotype resulting from the *cdc48-3* mutation. We note that the *cdc48-3* mutation reportedly arrests the cell cycle at metaphase, with large buds containing short spindles [44]. Therefore, the observed changes in the levels of metabolites could be, at least partially, correlated with the cell cycle phenotype of *cdc48-3* mutant cells [45].

Systematic analyses of ubiquitin modification in yeast have revealed that numerous metabolic enzymes are ubiquitinated, although their half-lives are not necessarily short under normal growth conditions. For example, ~19 out of ~25 enzymes in the glycolytic/gluconeogenic pathway and ~16 out of ~22 enzymes in the ergosterol synthetic pathway, are ubiquitinated in yeast, although they are mostly long-lived proteins [46–49] (www.yeastgenome.com). Therefore, one possibility would be that Cdc48 regulates the assembly and activity of metabolic enzymes via the ubiquitin chains attached to them. Although this study demonstrated a global cellular metabolic change upon Cdc48 inactivation, the individual action of Cdc48 on each ubiquitinated metabolic enzymes, particularly how its segregase activity regulates the formation of metabolic enzyme complexes, will need to be further clarified.

In the glycolytic pathway in *cdc48-3* cells, the intermediate metabolites above dihydroxyacetone phosphate (DHAP) were upregulated (e.g., glucose-6-phosphate, fructose-1,6-bisphosphate, and glyceraldehyde 3-phosphate), whereas the ones below DHAP in the pathway were downregulated (e.g., 3-phosphoglycerate, 2-phosphoglycerate, and phosphoenolpyruvate) (Fig. 2C). This typically happens when Hog1 (p38-related stress-activated protein kinase) is activated, which results in the intermediates of glycolysis (after DHAP) being diverted towards glycerol synthesis [50]. It is currently unknown if the non-functional Cdc48 alters the Hog1 activity. However, it should be noted that Ubp3 deubiquitinating enzyme, a known interactor of Cdc48, binds to Hog1, and its activity is regulated by the Hog1-mediated phosphorylation [51]. In this manner, metabolic changes observed in *cdc48-3* cells may not be associated with the Cdc48 loss of function but may be associated with the gain of function of one of its binding partners through a more indirect route. Thus, many individual possible mechanisms may exist for the metabolomics changes in *cdc48-3* cells.

In *cdc48-3* yeast cells, the levels of most amino acids decreased. This is probably because Cdc48 inhibition reduces proteasomal degradation, resulting in the generation of fewer amino acids as degradation products. This idea is consistent with the observation that proteasomal inhibition decreases the intracellular amino acid pool [52,53]. Interestingly, in mammals, treatment of cells with CB5083, a potent and selective inhibitor of p97/VCP [54], causes significant increases in the levels of most amino acids [55]. The explanation for this observation was that p97/VCP inhibition has a suppressive effect on *de novo* protein synthesis and, thus, amino acid usage [55]. As Cdc48/p97/VCP inhibition should have complex effects on protein synthesis, degradation, and metabolism, the exact reason for the

difference between results obtained in the *cdc48-3* yeast cells and in the CB5083-treated mammalian cells is currently unclear; however, accumulation of glutamine is likely a common consequence of inhibiting Cdc48 in yeast, and p97/VCP in mammals (Fig. 3) [55]. Regardless of the detailed mechanisms, p97/VCP regulates multiple cellular pathways, and its inhibition can be considered a promising anticancer drug target [52,55]. We suggest that metabolomic analyses of Cdc48-deficient yeast will be a complement to p97/VCP-related pathological and therapeutic studies.

Author contribution statement

Tomoyuki Kawarasaki: Performed the experiments.

Kunio Nakatsukasa: Conceived and designed the experiments; Performed the experiments; Analyzed and interpreted the data; Contributed reagents, materials, analysis tools or data; Wrote the paper.

Funding statement

Tomoyuki Kawarasaki was supported by JST SPRING. Kunio Nakatsukasa was supported by Toray Science Foundation and JSPS KAKENHI.

Data availability statement

Data included in article/supp. material/referenced in article.

Declaration of interest's statement

The authors declare that they have no known competing financial interests or personal relationships that could have appeared to influence the work reported in this paper.

Acknowledgments

We thank the members of the Nakatsukasa laboratory for discussion and critical comments on the manuscript.

Appendix A. Supplementary data

Supplementary data related to this article can be found at https://doi.org/10.1016/j.heliyon.2023.e13219.

References

[1] N. Bodnar, T. Rapoport, Toward an understanding of the Cdc48/p97 ATPase, F1000Res 6 (2017) 1318, https://doi.org/10.12688/f1000research.11683.1.
[2] N.O. Bodnar, T.A. Rapoport, Molecular mechanism of substrate processing by the Cdc48 ATPase complex, Cell 169 (2017) 722–735 e729, https://doi.org/10.1016/j.cell.2017.04.020.
[3] C. Schuberth, A. Buchberger, UBX domain proteins: major regulators of the AAA ATPase Cdc48/p97, Cell. Mol. Life Sci. 65 (2008) 2360–2371, https://doi.org/10.1007/s00018-008-8072-8.
[4] E.C. Twomey, Z. Ji, T.E. Wales, N.O. Bodnar, S.B. Ficarro, J.A. Marto, J.R. Engen, T.A. Rapoport, Substrate processing by the Cdc48 ATPase complex is initiated by ubiquitin unfolding, Science 365 (2019), https://doi.org/10.1126/science.aax1033.
[5] X. Wu, T.A. Rapoport, Mechanistic insights into ER-associated protein degradation, Curr. Opin. Cell Biol. 53 (2018) 22–28, https://doi.org/10.1016/j.ceb.2018.04.004.
[6] N. Berner, K.R. Reutter, D.H. Wolf, Protein quality control of the endoplasmic reticulum and ubiquitin-proteasome-triggered degradation of aberrant proteins: yeast pioneers the path, Annu. Rev. Biochem. 87 (2018) 751–782, https://doi.org/10.1146/annurev-biochem-062917-012749.
[7] D. Zattas, M. Hochstrasser, Ubiquitin-dependent protein degradation at the yeast endoplasmic reticulum and nuclear envelope, Crit. Rev. Biochem. Mol. Biol. 50 (2015) 1–17, https://doi.org/10.3109/10409238.2014.959889.
[8] K. Nakatsukasa, T. Kamura, Subcellular fractionation analysis of the extraction of ubiquitinated polytopic membrane substrate during ER-associated degradation, PLoS One 11 (2016), e0148327, https://doi.org/10.1371/journal.pone.0148327.
[9] K. Nakatsukasa, F. Okumura, T. Kamura, Proteolytic regulation of metabolic enzymes by E3 ubiquitin ligase complexes: lessons from yeast, Crit. Rev. Biochem. Mol. Biol. 50 (2015) 489–502, https://doi.org/10.3109/10409238.2015.1081869.
[10] J.O. Johnson, J. Mandrioli, M. Benatar, Y. Abramzon, V.M. Van Deerlin, J.Q. Trojanowski, J.R. Gibbs, M. Brunetti, S. Gronka, J. Wuu, J. Ding, L. McCluskey, M. Martinez-Lage, D. Falcone, D.G. Hernandez, S. Arepalli, S. Chong, J.C. Schymick, J. Rothstein, F. Landi, Y.D. Wang, A. Calvo, G. Mora, M. Sabatelli, M. R. Monsurro, S. Battistini, F. Salvi, R. Spataro, P. Sola, G. Borghero, I. Consortium, G. Galassi, S.W. Scholz, J.P. Taylor, G. Restagno, A. Chio, B.J. Traynor, Exome sequencing reveals VCP mutations as a cause of familial ALS, Neuron 68 (2010) 857–864, https://doi.org/10.1016/j.neuron.2010.11.036.
[11] G.D. Watts, J. Wymer, M.J. Kovach, S.G. Mehta, S. Mumm, D. Darvish, A. Pestronk, M.P. Whyte, V.E. Kimonis, Inclusion body myopathy associated with Paget disease of bone and frontotemporal dementia is caused by mutant valosin-containing protein, Nat. Genet. 36 (2004) 377–381, https://doi.org/10.1038/ng1332.
[12] V.E. Kimonis, E. Fulchiero, J. Vesa, G. Watts, VCP disease associated with myopathy, Paget disease of bone and frontotemporal dementia: review of a unique disorder, Biochim. Biophys. Acta 1782 (2008) 744–748, https://doi.org/10.1016/j.bbadis.2008.09.003.
[13] R. Higgins, M.H. Kabbaj, D. Sherwin, L.A. Howell, A. Hatcher, R.J. Tomko Jr., Y. Wang, The Cdc48 complex alleviates the cytotoxicity of misfolded proteins by regulating ubiquitin homeostasis, Cell Rep. 32 (2020), 107898, https://doi.org/10.1016/j.celrep.2020.107898.

[14] D. Xia, W.K. Tang, Y. Ye, Structure and function of the AAA+ ATPase p97/Cdc48p, Gene 583 (2016) 64–77, https://doi.org/10.1016/j.gene.2016.02.042.
[15] J. van den Boom, H. Meyer, VCP/p97-Mediated unfolding as a principle in protein homeostasis and signaling, Mol. Cell 69 (2018) 182–194, https://doi.org/10.1016/j.molcel.2017.10.028.
[16] J.M. Heo, N. Livnat-Levanon, E.B. Taylor, K.T. Jones, N. Dephoure, J. Ring, J. Xie, J.L. Brodsky, F. Madeo, S.P. Gygi, K. Ashrafi, M.H. Glickman, J. Rutter, A stress-responsive system for mitochondrial protein degradation, Mol. Cell 40 (2010) 465–480, https://doi.org/10.1016/j.molcel.2010.10.021.
[17] M.T. Hsieh, R.H. Chen, Cdc48 and cofactors Npl4-Ufd1 are important for G1 progression during heat stress by maintaining cell wall integrity in Saccharomyces cerevisiae, PLoS One 6 (2011), e18988, https://doi.org/10.1371/journal.pone.0018988.
[18] K. Cao, R. Nakajima, H.H. Meyer, Y. Zheng, The AAA-ATPase Cdc48/p97 regulates spindle disassembly at the end of mitosis, Cell 115 (2003) 355–367, https://doi.org/10.1016/s0092-8674(03)00815-8.
[19] A. Stolz, W. Hilt, A. Buchberger, D.H. Wolf, Cdc48: a power machine in protein degradation, Trends Biochem. Sci. 36 (2011) 515–523, https://doi.org/10.1016/j.tibs.2011.06.001.
[20] R. Verma, R.S. Oania, N.J. Kolawa, R.J. Deshaies, Cdc48/p97 promotes degradation of aberrant nascent polypeptides bound to the ribosome, Elife 2 (2013), e00308, https://doi.org/10.7554/eLife.00308.
[21] J.L. Yen, K. Flick, C.V. Papagiannis, R. Mathur, A. Tyrrell, I. Ouni, R.M. Kaake, L. Huang, P. Kaiser, Signal-induced disassembly of the SCF ubiquitin ligase complex by Cdc48/p97, Mol. Cell 48 (2012) 288–297, https://doi.org/10.1016/j.molcel.2012.08.015.
[22] K.W. Lin, K.R. McDonald, A.J. Guise, A. Chan, I.M. Cristea, V.A. Zakian, Proteomics of yeast telomerase identified Cdc48-Npl4-Ufd1 and Ufd4 as regulators of Est1 and telomere length, Nat. Commun. 6 (2015) 8290, https://doi.org/10.1038/ncomms9290.
[23] L. Stach, P.S. Freemont, The AAA+ ATPase p97, a cellular multitool, Biochem. J. 474 (2017) 2953–2976, https://doi.org/10.1042/BCJ20160783.
[24] C. Dargemont, B. Ossareh-Nazari, Cdc48/p97, a key actor in the interplay between autophagy and ubiquitin/proteasome catabolic pathways, Biochim. Biophys. Acta 1823 (2012) 138–144, https://doi.org/10.1016/j.bbamcr.2011.07.011.
[25] K. Nakatsukasa, T. Nishimura, S.D. Byrne, M. Okamoto, A. Takahashi-Nakaguchi, H. Chibana, F. Okumura, T. Kamura, The ubiquitin ligase SCF(Ucc1) acts as a metabolic switch for the glyoxylate cycle, Mol. Cell 59 (2015) 22–34, https://doi.org/10.1016/j.molcel.2015.04.013.
[26] K. Nakatsukasa, J.L. Brodsky, T. Kamura, A stalled retrotranslocation complex reveals physical linkage between substrate recognition and proteasomal degradation during ER-associated degradation, Mol. Biol. Cell 24 (2013) 1765–1775, https://doi.org/10.1091/mbc.E12-12-0907. S1761-1768.
[27] R.S. Sikorski, P. Hieter, A system of shuttle vectors and yeast host strains designed for efficient manipulation of DNA in Saccharomyces cerevisiae, Genetics 122 (1989) 19–27.
[28] K. Nakatsukasa, G. Huyer, S. Michaelis, J.L. Brodsky, Dissecting the ER-associated degradation of a misfolded polytopic membrane protein, Cell 132 (2008) 101–112, https://doi.org/10.1016/j.cell.2007.11.023.
[29] K. Nakatsukasa, M. Fujisawa, X. Yang, T. Kawarasaki, F. Okumura, T. Kamura, Triacylglycerol lipase Tgl4 is a stable protein and its dephosphorylation is regulated in a cell cycle-dependent manner in Saccharomyces cerevisiae, Biochem. Biophys. Res. Commun. 626 (2022) 85–91, https://doi.org/10.1016/j.bbrc.2022.08.022.
[30] K. Nakatsukasa, T. Kawarasaki, A. Moriyama, Heterologous expression and functional analysis of the F-box protein Ucc1 from other yeast species in Saccharomyces cerevisiae, J. Biosci. Bioeng. 128 (2019) 704–709, https://doi.org/10.1016/j.jbiosc.2019.06.003.
[31] Y. Ohashi, A. Hirayama, T. Ishikawa, S. Nakamura, K. Shimizu, Y. Ueno, M. Tomita, T. Soga, Depiction of metabolome changes in histidine-starved Escherichia coli by CE-TOFMS, Mol. Biosyst. 4 (2008) 135–147, https://doi.org/10.1039/b714176a.
[32] T. Ooga, H. Sato, A. Nagashima, K. Sasaki, M. Tomita, T. Soga, Y. Ohashi, Metabolomic anatomy of an animal model revealing homeostatic imbalances in dyslipidaemia, Mol. Biosyst. 7 (2011) 1217–1223, https://doi.org/10.1039/c0mb00141d.
[33] M. Sugimoto, D.T. Wong, A. Hirayama, T. Soga, M. Tomita, Capillary electrophoresis mass spectrometry-based saliva metabolomics identified oral, breast and pancreatic cancer-specific profiles, Metabolomics 6 (2010) 78–95, https://doi.org/10.1007/s11306-009-0178-y.
[34] B.H. Junker, C. Klukas, F. Schreiber, VANTED: a system for advanced data analysis and visualization in the context of biological networks, BMC Bioinf. 7 (2006) 109, https://doi.org/10.1186/1471-2105-7-109.
[35] M. Latterich, K.U. Frohlich, R. Schekman, Membrane fusion and the cell cycle: cdc48p participates in the fusion of ER membranes, Cell 82 (1995) 885–893, https://doi.org/10.1016/0092-8674(95)90268-6.
[36] S.M. Alberts, C. Sonntag, A. Schafer, D.H. Wolf, Ubx4 modulates cdc48 activity and influences degradation of misfolded proteins of the endoplasmic reticulum, J. Biol. Chem. 284 (2009) 16082–16089, https://doi.org/10.1074/jbc.M809282200.
[37] A. Decottignies, A. Evain, M. Ghislain, Binding of Cdc48p to a ubiquitin-related UBX domain from novel yeast proteins involved in intracellular proteolysis and sporulation, Yeast 21 (2004) 127–139, https://doi.org/10.1002/yea.1071.
[38] L. Barbin, F. Eisele, O. Santt, D.H. Wolf, The Cdc48-Ufd1-Npl4 complex is central in ubiquitin-proteasome triggered catabolite degradation of fructose-1,6-bisphosphatase, Biochem. Biophys. Res. Commun. 394 (2010) 335–341, https://doi.org/10.1016/j.bbrc.2010.03.005.
[39] R. Verma, R. Oania, R. Fang, G.T. Smith, R.J. Deshaies, Cdc48/p97 mediates UV-dependent turnover of RNA Pol II, Mol. Cell 41 (2011) 82–92, https://doi.org/10.1016/j.molcel.2010.12.017.
[40] C.Y. Chien, R.H. Chen, Cdc48 chaperone and adaptor Ubx4 distribute the proteasome in the nucleus for anaphase proteolysis, J. Biol. Chem. 288 (2013) 37180–37191, https://doi.org/10.1074/jbc.M113.513598.
[41] S.J. Remington, Structure and mechanism of citrate synthase, Curr. Top. Cell. Regul. 33 (1992) 209–229, https://doi.org/10.1016/b978-0-12-152833-1.50017-4.
[42] T.V. Nguyen, J. Li, C.J. Lu, J.L. Mamrosh, G. Lu, B.E. Cathers, R.J. Deshaies, p97/VCP promotes degradation of CRBN substrate glutamine synthetase and neosubstrates, Proc. Natl. Acad. Sci. U. S. A 114 (2017) 3565–3571, https://doi.org/10.1073/pnas.1700949114.
[43] J.C. Christianson, P. Carvalho, Order through destruction: how ER-associated protein degradation contributes to organelle homeostasis, EMBO J. 41 (2022), e109845, https://doi.org/10.15252/embj.2021109845.
[44] Y.L. Cheng, R.H. Chen, The AAA-ATPase Cdc48 and cofactor Shp1 promote chromosome bi-orientation by balancing Aurora B activity, J. Cell Sci. 123 (2010) 2025–2034, https://doi.org/10.1242/jcs.066043.
[45] L. Cai, B.P. Tu, Driving the cell cycle through metabolism, Annu. Rev. Cell Dev. Biol. 28 (2012) 59–87, https://doi.org/10.1146/annurev-cellbio-092910-154010.
[46] S. Back, A.W. Gorman, C. Vogel, G.M. Silva, Site-specific K63 ubiquitinomics provides insights into translation regulation under stress, J. Proteome Res. 18 (2019) 309–318, https://doi.org/10.1021/acs.jproteome.8b00623.
[47] N.N. Fang, G.T. Chan, M. Zhu, S.A. Comyn, A. Persaud, R.J. Deshaies, D. Rotin, J. Gsponer, T. Mayor, Rsp5/Nedd4 is the main ubiquitin ligase that targets cytosolic misfolded proteins following heat stress, Nat. Cell Biol. 16 (2014) 1227–1237, https://doi.org/10.1038/ncb3054.
[48] R. Christiano, N. Nagaraj, F. Frohlich, T.C. Walther, Global proteome turnover analyses of the Yeasts S. cerevisiae and S. pombe, Cell Rep. 9 (2014) 1959–1965, https://doi.org/10.1016/j.celrep.2014.10.065.
[49] R. Christiano, H. Arlt, S. Kabatnik, N. Mejhert, Z.W. Lai, R.V. Farese Jr., T.C. Walther, A systematic protein turnover map for decoding protein degradation, Cell Rep. 33 (2020), 108378, https://doi.org/10.1016/j.celrep.2020.108378.
[50] J.L. Brewster, M.C. Gustin, Hog1: 20 years of discovery and impact, Sci. Signal. 7 (2014) re7, https://doi.org/10.1126/scisignal.2005458.
[51] C. Sole, M. Nadal-Ribelles, C. Kraft, M. Peter, F. Posas, E. de Nadal, Control of Ubp3 ubiquitin protease activity by the Hog1 SAPK modulates transcription upon osmostress, EMBO J. 30 (2011) 3274–3284, https://doi.org/10.1038/emboj.2011.227.
[52] K. Parzych, T.M. Chinn, Z. Chen, S. Loaiza, F. Porsch, G.N. Valbuena, M.F. Kleijnen, A. Karadimitris, E. Gentleman, H.C. Keun, H.W. Auner, Inadequate fine-tuning of protein synthesis and failure of amino acid homeostasis following inhibition of the ATPase VCP/p97, Cell Death Dis. 6 (2015), e2031, https://doi.org/10.1038/cddis.2015.373.

[53] A. Suraweera, C. Munch, A. Hanssum, A. Bertolotti, Failure of amino acid homeostasis causes cell death following proteasome inhibition, Mol. Cell 48 (2012) 242–253, https://doi.org/10.1016/j.molcel.2012.08.003.

[54] D.J. Anderson, R. Le Moigne, S. Djakovic, B. Kumar, J. Rice, S. Wong, J. Wang, B. Yao, E. Valle, S. Kiss von Soly, A. Madriaga, F. Soriano, M.K. Menon, Z.Y. Wu, M. Kampmann, Y. Chen, J.S. Weissman, B.T. Aftab, F.M. Yakes, L. Shawver, H.J. Zhou, D. Wustrow, M. Rolfe, Targeting the AAA ATPase p97 as an approach to treat cancer through disruption of protein homeostasis, Cancer Cell 28 (2015) 653–665, https://doi.org/10.1016/j.ccell.2015.10.002.

[55] K. Parzych, P. Saavedra-Garcia, G.N. Valbuena, H.A. Al-Sadah, M.E. Robinson, L. Penfold, D.M. Kuzeva, A. Ruiz-Tellez, S. Loaiza, V. Holzmann, V. Caputo, D. C. Johnson, M.F. Kaiser, A. Karadimitris, E.W. Lam, E. Chevet, N. Feldhahn, H.C. Keun, H.W. Auner, The coordinated action of VCP/p97 and GCN2 regulates cancer cell metabolism and proteostasis during nutrient limitation, Oncogene 38 (2019) 3216–3231, https://doi.org/10.1038/s41388-018-0651-z.